

1 **Lidar vertical observation network and data assimilation reveal key**  
2 **processes driving the 3-D dynamic evolution of PM<sub>2.5</sub> concentrations over**  
3 **the North China Plain**

4 Yan Xiang<sup>1</sup>, Tianshu Zhang<sup>2, 1</sup>, Chaoqun Ma<sup>3</sup>, Lihui Lv<sup>1</sup>, Jianguo Liu<sup>2</sup>, Wenqing Liu<sup>2, 1</sup>, and  
5 Yafang Cheng<sup>3</sup>

6 <sup>1</sup>Institutes of Physical Science and Information Technology, Anhui University, Hefei 230601, China

7 <sup>2</sup>Key Laboratory of Environmental Optics and Technology, Anhui Institute of Optics and Fine  
8 Mechanics, Chinese Academy of Sciences, Hefei 230031, China

9 <sup>3</sup>Minerva Research Group, Max Planck Institute for Chemistry, Mainz, Germany

10 **Correspondence:** Yan Xiang (yxiang@ahu.edu.cn) and Yafang Cheng (yafang.cheng@mpic.de)

11 **Abstract:** China has made great efforts to monitor and control air pollution in the past decade.  
12 Comprehensive characterization and understanding of pollutants in three-dimension (3-D) are,  
13 however, still lacking. Here, we used data from an observation network consisting of 13 aerosol  
14 lidars and more than 1000 ground observation stations, combined with a data assimilation  
15 technique, to conduct a comprehensive analysis of an extreme heavy aerosol pollution (HAP)  
16 over the North China Plain (NCP) from November–December 2017. During the studied period,  
17 the maximum hourly mass concentration of surface PM<sub>2.5</sub> reached ~390 μg·m<sup>-3</sup>. After  
18 assimilation, the correlation between model results and the independent observation sub-  
19 dataset was ~50% higher than the that without the assimilation, and the root mean square error  
20 was reduced by ~40%. From pollution development to dissipation, we divided the HAP in the  
21 NCP (especially in Beijing) into four phases—an early phase (EP), a transport phase (TP), an  
22 accumulation phase (AP), and a removal phase (RP). We then analyzed the evolutionary  
23 characteristics of PM<sub>2.5</sub> concentration during different phases on the surface and in 3-D space.  
24 We found that the particles were mainly transported from south to north at a height of 1-2 km  
25 (during EP and RP) and near the surface (during TP and AP). The amounts of PM<sub>2.5</sub> advected  
26 into Beijing with the maximum transport flux intensity (TFI) were through the pathways in the  
27 relative order of the southwest > southeast > east pathways. The dissipation of PM<sub>2.5</sub> in the RP  
28 stage (with negative TFI) was mainly from north to south, with an average transport height of  
29 ~1 km above the surface. Our results quantified the multi-dimensional distribution and  
30 evolution of PM<sub>2.5</sub> concentration over the NCP, which may help policymakers develop efficient  
31 air pollution control strategies.

## 1 **1 Introduction**

2 Frequent heavy air pollution has exerted significant impacts on air visibility, climate,  
3 human health, and other environmental concerns (Gao, Woodward, et al. 2017; Pokharel et al.  
4 2019; Su, Cheng, and Poschl 2020). As a developing country with the largest population in the  
5 world, China's air quality has exhibited an obvious improvement trend in recent years (Zhang  
6 and Cao 2015; Cao et al. 2017). Regional air pollution in China is still serious, however,  
7 especially the heavy aerosol pollution (HAP) caused by fine particulate matter (PM<sub>2.5</sub>) in winter,  
8 which has attracted attention worldwide (Zheng et al. 2019; Li, Zhang, et al. 2017; Zheng et al.  
9 2015; Cheng et al. 2016). Therefore, providing a reliable distribution of the PM<sub>2.5</sub> concentration  
10 of HAP, especially at any time and at any height in a given region, is particularly important in  
11 the quest of the public to avoid health problems and to provide government policy makers with  
12 help in designing effective controls (Hu et al. 2015).

13 Compared with other air pollutants (e.g., ozone and nitrogen dioxide), PM<sub>2.5</sub> has a longer  
14 atmospheric lifetime (3–5 days), during which it can be transported vertically to great heights  
15 and horizontally hundreds of kilometers (Wang et al. 2017; Zhang et al. 2014), depending on  
16 the meteorological conditions (e.g., relative humidity and precipitation) and chemical  
17 composition (Yang et al. 2017). Previous study demonstrated that regional transport plays an  
18 important role for pollution formation in major cities of China, e.g., transport contributes over  
19 50% of the PM<sub>2.5</sub> mass concentration in Beijing city, Shanghai city, Hangzhou city, Guangzhou  
20 city, Hong Kong and Chengdu city during the relatively polluted period (Sun et al. 2017). From  
21 2005–2010, annually, about 35.5% (32.8  $\mu\text{g}\cdot\text{m}^{-3}$ ) of the PM<sub>2.5</sub> in Beijing was attributed to  
22 regional transport from the North China Plain (NCP), within which up to 60.4% (64.3  $\mu\text{g}\cdot\text{m}^{-3}$ )  
23 from southerly and westerly air flows (Wang et al. 2015). Since the 2013 implementation of  
24 the most stringent clean air policy in China, the control of local pollution sources has led to the  
25 rapid reduction of total PM<sub>2.5</sub> concentration (Zhang, Zheng, et al. 2019). It should be noted,  
26 however, that the local contributions, intra-regional transport, and inter-regional transport  
27 accounted for 47% (12.7  $\mu\text{g}\cdot\text{m}^{-3}$ ), 25% (6.6  $\mu\text{g}\cdot\text{m}^{-3}$ ), and 28% (7.6  $\mu\text{g}\cdot\text{m}^{-3}$ ), respectively, of the  
28 total PM<sub>2.5</sub> for the Beijing-Tianjin-Hebei (BTH) region from 2014–2017, with the 2017  
29 contribution of regional transport to the BTH concentration rate ranging from 32.5–68.4%  
30 (Dong et al. 2020).

31 Previous studies have shown that it is difficult to use surface observations to characterize  
32 the impact of upper-level pollutants in the atmosphere (Huang, Wang, and Ding 2018), which  
33 is affected by local emissions, regional transport, meteorological conditions, geographical

1 factors etc. (Tao et al. 2020; Che, Gui, et al. 2019). Therefore, understanding the key processes  
2 that drive the dynamic temporal and spatial evolutionary characteristics of pollutants on the  
3 NCP is essential for revealing the source and transport of aerosols, which has different radiative  
4 forcing at different heights (Kumar et al. 2017; Che, Xia, et al. 2019). Actually, stereo-  
5 monitoring devices and technologies, such as lidar (Sheng et al. 2019; Fan et al. 2019; Chen,  
6 Schofield, et al. 2019), MAX-DOAS (Hong et al. 2018; Zhang et al. 2020), and satellite remote  
7 sensing (Pang et al. 2018; Schwartz et al. 2012; Zhang, Liu, et al. 2019), can reveal the vertical  
8 distribution of pollutants at different heights (Tian et al. 2017; Heese et al. 2017). Due to the  
9 limited spatial and temporal observations, however, it is impossible to provide physical and  
10 chemical properties in the atmosphere at any time period and on any path, which makes it  
11 difficult to directly reveal the formation and source of pollution.

12 On the other hand, although the distribution of pollutants can be simulated by air quality  
13 models (Huang et al. 2018; Zhang et al. 2008), large uncertainties remain, mainly from the  
14 influence of emission inventory, meteorological fields, and some hypothetical conditions (Xu  
15 et al. 2016; Chen et al. 2017; Huang et al. 2016). Fortunately, the above observed data and the  
16 results of the model can be fused using data assimilation techniques, which can correct the  
17 model simulation results via the observed data (Wang et al. 2013; Ma et al. 2019). Research  
18 has shown that mainstream data assimilation (DA) technologies, including 3DVAR (Jiang et  
19 al. 2013; Ma et al. 2018), 4DVAR (Yumimoto et al. 2008), and EnKF (Chen, Liu, et al. 2019),  
20 can be used to assimilate observation data from the surface, remote sensing data (such as AOD)  
21 from satellites, and vertical profile data from lidar, all of which can be used to improve the  
22 performance of the model, including the simulation of  $PM_{2.5}$  and  $PM_{10}$ .

23 In this study, we analyzed the observation data from a vertical observation network  
24 consisting of 13 lidars and surface observation stations during an extreme pollution event in  
25 eastern China, especially in the NCP. Next, all of the data were utilized by the Gridpoint  
26 Statistical Interpolation (GSI) three-dimensional (3-D) variational (3DVAR) data assimilation  
27 system to revise the  $PM_{2.5}$  results from the WRF-Chem simulation (Pagowski et al. 2014).  
28 Finally, the multi-dimensional evolutionary characteristics of  $PM_{2.5}$  at the surface and in the  
29 vertical layer, as well as the 3-D distribution, were analyzed in detail. Although data  
30 assimilation has been applied in China using surface observation network data (Gao, Saide, et  
31 al. 2017), AOD (Saide et al. 2014; Saide et al. 2013; Schwartz et al. 2012; Liu et al. 2011), and  
32 lidar data (Cheng et al. 2019), to our knowledge, this is the first attempt in China to apply lidar  
33 network data to assimilation technology, from which the high-precision 3-D distribution of

1 pollutants can be provided, thus supplying effective data support for clarifying the formation  
2 mechanism of pollutants (Zheng et al. 2017).

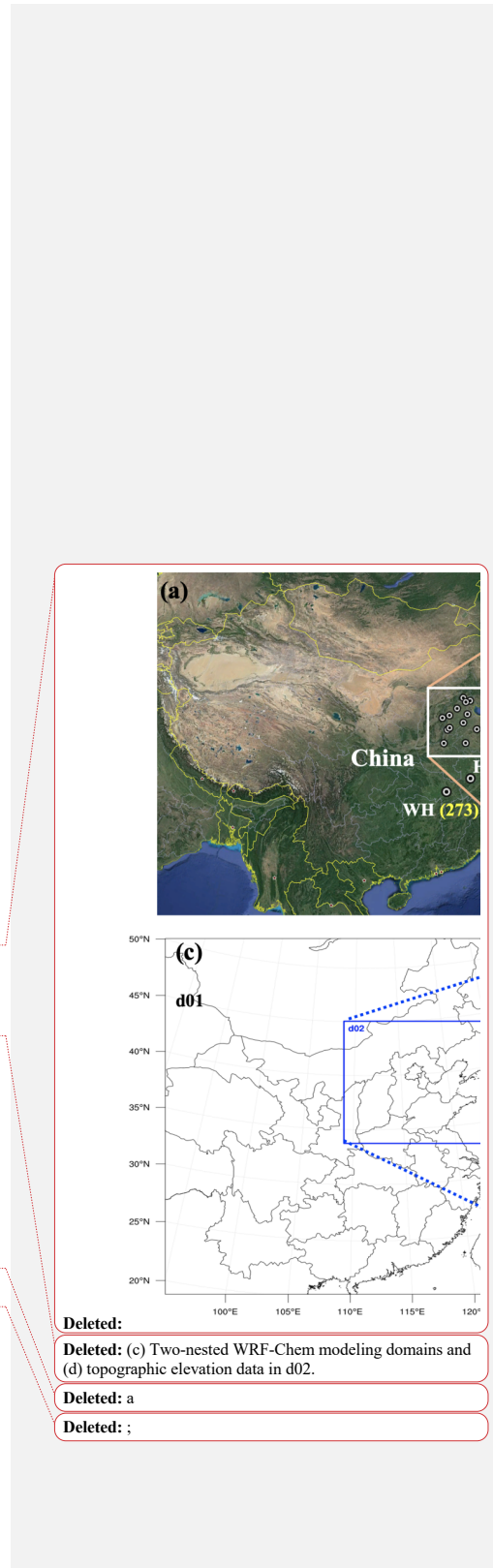
## 3 2 Measurements and methods

### 4 2.1 Lidar observation network

5 The vertical aerosol observation network of the NCP was composed of 13 aerosol lidar  
6 monitoring stations (Fig. 1), covering four main transport channels of Beijing pollutants,  
7 including the southwestern transport path of Baoding City (BD), Shijiazhuang City (SJZ),  
8 Xingtai City (XT), Handan City (HD), Xinxiang City (XX), and Yangquan City (YQ); the  
9 southern transport path of Dezhou City (DZ) and Jining City (JN); the southeastern transport  
10 path of Langfang City (LF), Cangzhou City (CZ), and Zibo City (ZB); the eastern transport  
11 path of Tianjin City (TJ); and a lidar in the urban area of Beijing (BJ).

12  
13 **Figure 1.** © Google maps of (a) China with the studied cities and (b) the North China Plain with all the  
14 lidar stations. The data in brackets are the maximum PM<sub>2.5</sub> concentrations ( $\mu\text{g}\cdot\text{m}^{-3}$ ) at the surface during  
15 the observation period. The black arrows in (b, d) from left to right show that the main pollution  
16 pathways of Beijing come from the four directions of southwest, south, southeast, and east.

17 The lidar system was developed by the Anhui Institute of Optics and Fine Mechanics  
18 (AIOFM), Chinese Academy of Sciences (CAS), and was used for the long-term continuous  
19 observation of aerosol vertical distribution. The lidar system adopted the Nd: YAG laser, which  
20 emits a 532-nm wavelength, with 30-mJ single-pulse energy and 10–30-Hz pulse repetition  
21 frequency. The vertical resolution is 7.5 m, with the original time resolution of 3–10 min. The  
22 detection blind area is 0.1 km, and more specific technical details can be found in other  
23 literature (Xiang et al. 2019). The vertical distribution of the aerosol extinction coefficient was  
24 retrieved using the Fernald method (Fernald 1984), which is more suitable for vertical detection  
25 and more accurate than the Collis (Collis, Fernald, and Ligda 1964) and Klett (Klett 1981)



Deleted:  
Deleted: (c) Two-nested WRF-Chem modeling domains and  
Deleted: (d) topographic elevation data in d02.  
Deleted: a  
Deleted: ;



1 methods (Lu et al. 2015). Furthermore, combining the extinction coefficient with the PM<sub>2.5</sub> *in-*  
2 *situ* surface observations, the vertical distribution of the PM<sub>2.5</sub> mass concentration in the  
3 boundary layer was obtained using the empirical formula fitting method, which has proven to  
4 be reliable and highly accurate; the specific technical details can be found in other literature  
5 (Lv et al. 2017b; Tao et al. 2016; Lv et al. 2017a). In addition, an image recognition algorithm  
6 was used to evaluate the height of the atmospheric boundary layer (Xiang et al. 2019; Barrera  
7 et al. 2019).

## 8 **2.2 WRF-Chem model configurations**

9 The WRF-Chem chemical transport model (version 3.8.1) was used to investigate the  
10 particulate concentrations and meteorological parameters in the study area and was configured  
11 with nested domains consisting of 100 × 100 (36 km) and 103 × 103 (12 km) grids (Figs. S1).  
12 The domain had 41 vertical layers from the surface to 50 hPa. To better simulate the conditions  
13 within the boundary layer, the resolution of the boundary layer was increased, and 20 layers  
14 were set in the range of 0–2 km. The initial and boundary meteorological conditions were  
15 derived from the 6-h National Centers for Environmental Prediction Final Analysis data with  
16 1° × 1° spatial resolution. The inventory of anthropogenic emissions for 2016 was obtained  
17 from the Multi-resolution Emission Inventory for China (MEIC) data with 0.25° × 0.25°  
18 resolution (Zhou et al. 2017). Terrestrial biogenic emissions were estimated using the Model  
19 of Emissions of Gases and Aerosols from Nature (MEGAN) model (Chatani et al. 2011). The  
20 gas-phase chemistry module CBM-Z and the Model for Simulating Aerosol Interactions and  
21 Chemistry (MOSAIC) aerosol module were used in this simulation. Detailed information  
22 concerning the model configuration is provided in Table S1. The model runs from November  
23 20, 2017–December 9, 2017, and the results from November 25–December 9, 2017 were used  
24 for the analysis in Section 3.

## 25 **2.3 GSI 3DVAR DA system**

26 The GSI DA (Gridpoint Statistical Interpolation Data Assimilation) system provides  
27 3DVAR analysis by minimizing the cost function as shown below (Gao, Saide, et al. 2017):

$$28 \quad J(x) = (x - x_b)^T B^{-1} (x - x_b) + (y - H(x))^T R^{-1} (y - H(x)) \quad (1)$$

29 In this equation,  $x$  is the analysis vector,  $x_b$  denotes the background vector,  $y$  is an observation  
30 vector,  $B$  represents the background error covariance matrix,  $R$  represents the observation error  
31 covariance matrix, and  $H$  is the observation operator used to transform model grid point values  
32 to observed variables, which was performed via interpolation in our research. The background  
33 error covariance matrix was calculated using the National Meteorological Center (NMC)

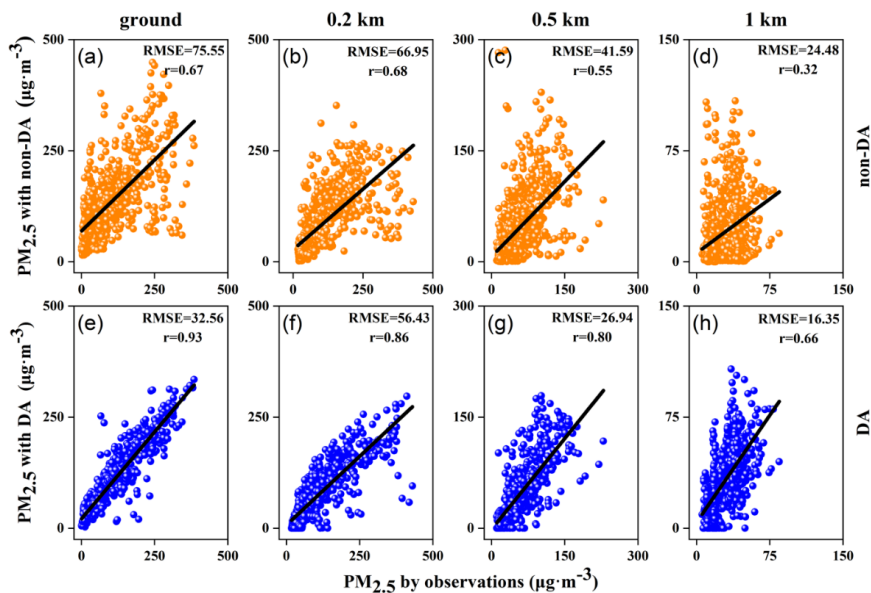
Deleted: 1c and 1d

1 method (Parrish and Derber 1992; Saide et al. 2013), which simulated the difference of results  
2 at the same time (November 25, 2017) with two different starting times (November 20, 2017  
3 and November 21, 2017, respectively). The 1-hour assimilated window data included 13  
4 groups (see Fig. 1 for site distribution) of PM<sub>2.5</sub> vertical profiles retrieved from lidar, and the  
5 surface PM<sub>2.5</sub> data from hundreds of surface monitoring stations (see Fig. 5 for site distribution)  
6 from the China Environmental Monitoring Center. The observation errors of PM<sub>2.5</sub> ground and  
7 its vertical distribution (through the ground PM<sub>2.5</sub> fitting method in Section 2.1) originated  
8 from measurement errors and representative errors. The measurement error was computed  
9 using  $\varepsilon_0 = 1.5 + 0.0075 * obs$  (Pagowski et al. 2014), where *obs* indicates observed values.  
10 The representative error was computed using  $\varepsilon_r = \gamma \varepsilon_0 \sqrt{\Delta x / L}$  (Elbern et al. 2007), where  $\gamma$  is  
11 the adjustable scale factor (we used the value of 0.5 recommended by the GSI system),  $\Delta x$  is  
12 the model grid resolution (we selected 12 km of domain 2), and  $L$  is the influencing radius (we  
13 used 60 km).

### 14 **3 Results and discussion**

#### 15 **3.1 Evaluation of assimilation performance using vertical PM<sub>2.5</sub> data**

16 In order to evaluate the improvement of model simulation performance from data  
17 assimilation using lidar vertical profile data and surface station data, considering the sharp  
18 decline of PM<sub>2.5</sub> value at 1 km height (Fig. 6), only the non-assimilation and assimilation results  
19 at the surface, 0.2 km, 0.5 km, and 1 km were compared, as shown in Fig. 2. These data were  
20 selected from five of the most polluted stations, including the cities of TJ, LF, BD, SJZ, and  
21 XT. It should be noted that these observation data were not assimilated, which means that the  
22 following comparisons are independent (Bocquet et al. 2015). Obviously, the data assimilation  
23 used can greatly improve the simulation accuracy. Compared with the observation data at  
24 different heights (**ground, 0.2, 0.5 and 1 km**), the simulation results of PM<sub>2.5</sub> levels under the  
25 condition of non-assimilation were higher (Figs. 2 a–d), the root-mean-square error (RMSE)  
26 was  $52.14 \pm 20.27 \mu\text{g}\cdot\text{m}^{-3}$ , and the correlation coefficient was only  $0.56 \pm 0.15$ .  
27 Correspondingly, the results of PM<sub>2.5</sub> simulated with assimilation were closer to the observed  
28 values (Figs. 2 e–h), the RMSE was  $33.07 \pm 14.69 \mu\text{g}\cdot\text{m}^{-3}$ , which represents a reduction of  
29 about 40% in simulation error after assimilation. The correlation coefficient was  $0.81 \pm 0.10$ ,  
30 demonstrating that the simulation accuracy was improved by about 50% after assimilation.



1  
2 **Figure 2.** PM<sub>2.5</sub> mass concentration comparison results from lidar at different heights (b–d, f–h) and  
3 surface observations (a, e) with non-assimilation simulations (a–d) and assimilation simulations (e–h).

4 In addition, compared with the simulation with assimilation (Fig. 5 in Section 3.3), the  
5 results without assimilation were significantly higher than the observed values (Fig. S2),  
6 especially during the pollution period (Figs. S2d, S2e), which may be due to the simulation  
7 error caused by the model (Zhang et al. 2016). Meanwhile, the comparison of the three-  
8 dimensional results (Fig. 7 in Section 3.5 and Fig. S3) further reveals that the simulation results  
9 of upper air PM<sub>2.5</sub> may also overestimate the actual values, which demonstrates the importance  
10 of data assimilation in capturing the three-dimensional structure of pollution.

### 11 3.2 The four phases from aerosol pollution development to dissipation

12 Joint observations and analyses have been widely performed in an effort to reveal the  
13 heavy aerosol pollution (HAP) in the NCP region (Li et al. 2016; Zhang et al. 2018). The key  
14 processes of a HAP event, from aerosol pollution development to dissipation, usually include  
15 an early phase (EP), a transport phase (TP), an accumulation phase (AP), and a removal phase  
16 (RP) (Yuan et al. 2019; Zhong et al. 2017), classifications that are based on the increase and  
17 decrease of PM<sub>2.5</sub> mass concentration in Beijing (BJ) caused by changes in meteorological  
18 conditions. Here, the curves in Fig. 3 shows the temporal evolution of PM<sub>2.5</sub> mass concentration  
19 monitored at the surface in different cities on the NCP from November 25–December 9, 2017,

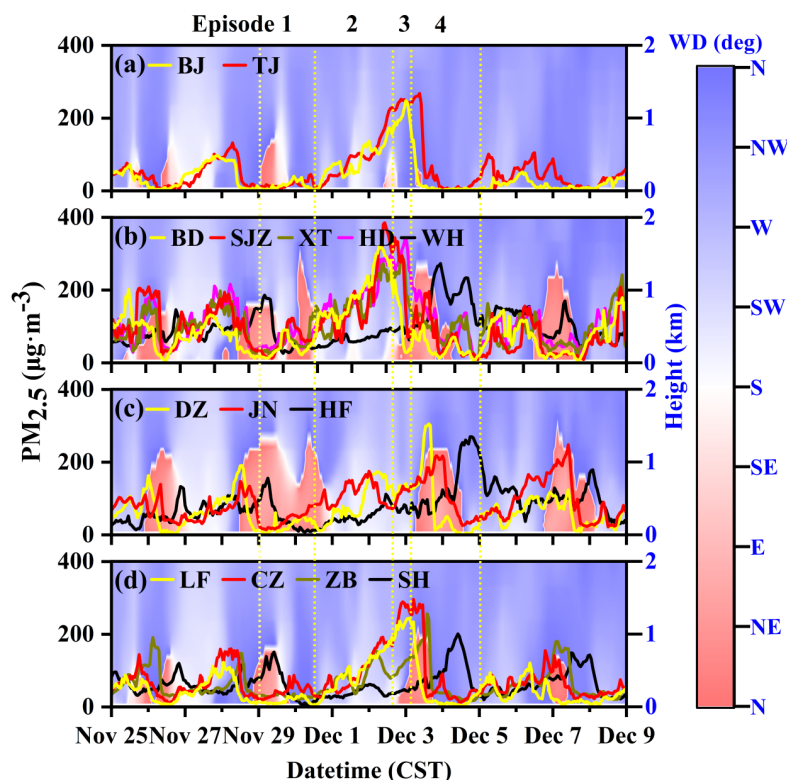
Deleted: S1

Deleted: S1d

Deleted: S1e

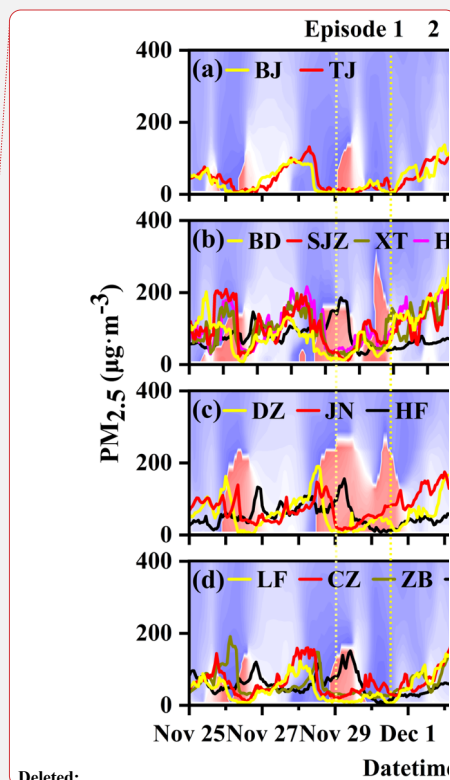
Deleted: S2

1 while the superimposed colors represent the time-varying profiles of the simulated wind fields  
 2 in BJ, Baoding (BD), Dezhou (DZ), and Langfang (LF), respectively. Overall,  $PM_{2.5}$  with high  
 3 concentrations was usually associated with pronounced southerly winds (S in Fig. 3) or  
 4 southwesterly winds (SW in Fig. 3), while the  $PM_{2.5}$  concentrations decreased significantly  
 5 under the prevailing northerly winds (including the wind directions of N, NW, and NE in Fig.  
 6 3).



7  
 8 **Figure 3.** Surface  $PM_{2.5}$  observations from different cities: (a) Beijing (including Tianjin) and its (b)  
 9 southwest cities, (c) southeast cities, and (d) east cities for the period November 25–December 9, 2017.  
 10 Superimposed colors represent the time-varying profiles of the simulated wind fields in Beijing,  
 11 Baoding, Dezhou, and Langfang, respectively.

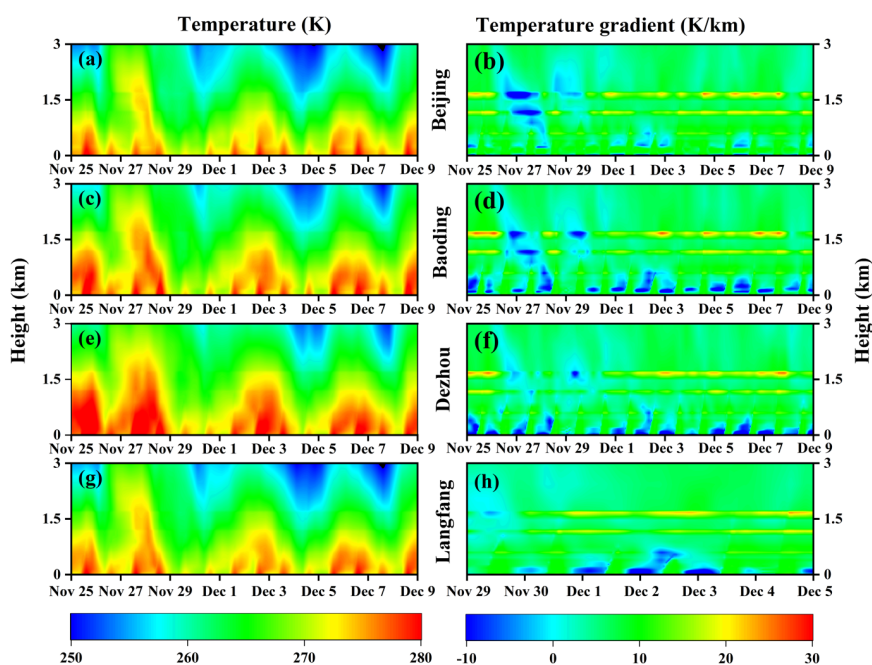
12 Furthermore, in order to characterize the evolution of  $PM_{2.5}$  during different pollution  
 13 phases, the period from November 29–December 5 was selected as a typical extreme HAP  
 14 event covering the four pollution phases. This extreme pollution event lasted more than 4 days  
 15 and featured a regional transport process. During the EP (November 29–noon November 30;



1 episode 1 in Fig. 3), the air quality in BJ and its surrounding areas such as Tianjin (TJ) was  
2 relatively good, with an average  $PM_{2.5}$  value of  $\sim 15 \mu\text{g}\cdot\text{m}^{-3}$ , while slight pollution occurred to  
3 the southwest of BJ, including BD, Shijiazhuang (SJZ), Xingtai (XT), and Handan (HD), with  
4 an average value of  $\sim 50 \mu\text{g}\cdot\text{m}^{-3}$ .

5 During the TP (approximately the morning of December 2; episode 2 in Fig. 3), the  
6 variation of  $PM_{2.5}$  concentration was more sensitive and responded rapidly to the wind shift  
7 from northerly to southerly, causing the  $PM_{2.5}$  concentration in Beijing to increase quickly from  
8  $\sim 30 \mu\text{g}\cdot\text{m}^{-3}$  to  $\sim 150 \mu\text{g}\cdot\text{m}^{-3}$ , while southwest of Beijing (e.g., BD, SJZ, XT, and HD) the  $PM_{2.5}$   
9 concentration increased rapidly to  $\sim 200 \mu\text{g}\cdot\text{m}^{-3}$ . Research has revealed that the pollutant  
10 transport south of Beijing, especially in the southwest areas (the Taihang Mountains), is the  
11 most important contribution source of Beijing pollutants (Zhao et al. 2020). During the AP  
12 (approximately December 3; episode 3 in Fig. 3), diffusion of the pollutants was difficult due  
13 to the occurrence of a surface temperature inversion in Beijing (Fig. 4) (Wang et al. 2019),  
14 which caused the maximum concentration of  $PM_{2.5}$  in Beijing to reach  $\sim 250 \mu\text{g}\cdot\text{m}^{-3}$ .  
15 Meanwhile, the  $PM_{2.5}$  concentrations in TJ, LF, BD, and SJZ reached maximum values of  $\sim 270$ ,  
16 250, 320, and  $390 \mu\text{g}\cdot\text{m}^{-3}$ , respectively. Conversely, the pollution levels in Shanghai (SH),  
17 Hefei (HF), and Wuhan (WH) in the southernmost section of the NCP were relatively low,  
18 with average values  $< \sim 60 \mu\text{g}\cdot\text{m}^{-3}$ .

19 During the RP (approximately December 5; episode 4 in Fig. 3), the wind direction  
20 shifted from southwest to north, transporting the relatively clean air in the north to the south,  
21 and thereby causing the pollutant concentrations in Beijing to decrease rapidly. In just 9 hours,  
22 the air quality improved from heavy pollution to excellent, and the  $PM_{2.5}$  concentrations in the  
23 NCP also decreased significantly. Finally, by noon on December 4, the pollutant concentrations  
24 in the NCP had reached a low level, with an average value of  $\sim 40 \mu\text{g}\cdot\text{m}^{-3}$ . In contrast, due to  
25 the continuous southward advection of pollutants, serious pollution occurred in SH, HF, and  
26 WH, where the  $PM_{2.5}$  concentrations reached maximum values of  $\sim 210$ , 310, and  $280 \mu\text{g}\cdot\text{m}^{-3}$ ,  
27 respectively. These findings are also consistent with the results of previous studies on the  
28 regional transport of regional pollutants to the Yangtze River Delta (Hua et al. 2015), which  
29 showed them to be due to the continuous southward flow of northwest and northeast winds.



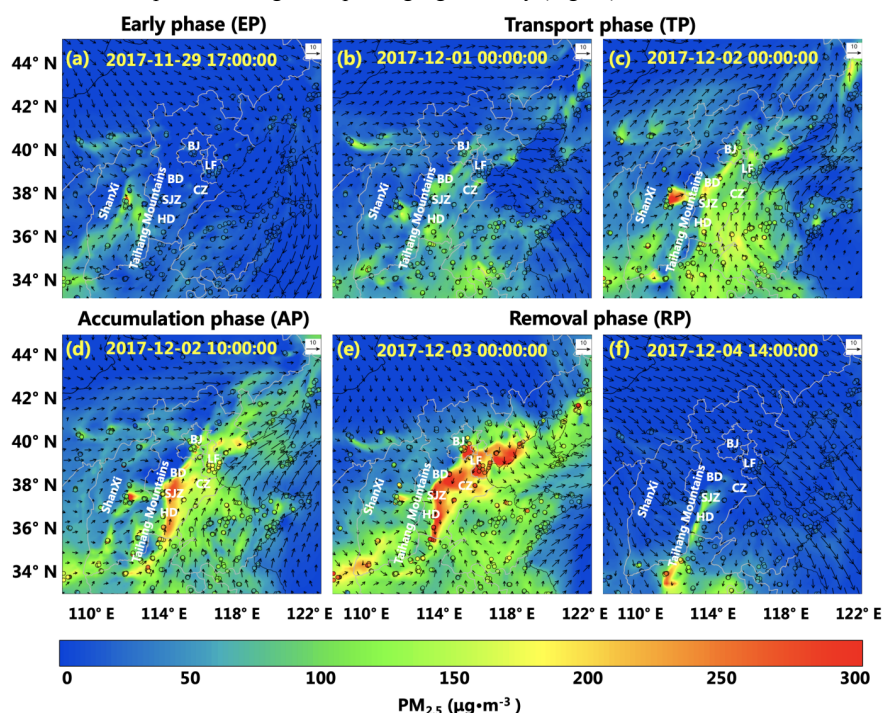
1  
2 **Figure 4.** Time series of vertical temperatures (a, c, e, g) and temperature gradients (b, d, f, h) from  
3 Beijing (a, b), Baoding (c, d), Dezhou (e, f), and Langfang (g, h) simulated by the WRF-Chem model.

### 4 3.3 Spatial distribution of PM<sub>2.5</sub> concentration in the surface layer

5 Additionally, in order to analyze the pollution characteristics of the NCP, the spatial  
6 distribution results of PM<sub>2.5</sub> after data assimilation were plotted in Fig. 5 for all phases. The  
7 high concentrations of PM<sub>2.5</sub> in BJ were recorded during the TP, AP, and beginning of the RP,  
8 while the PM<sub>2.5</sub> concentrations at other times were lower. Moreover, during the EP, only the  
9 eastern cities of Shanxi (SX) Province experienced moderate pollution levels (Fig. 5a). During  
10 the TP, the pollutants in the south-central NCP were transported to the north of the NCP (Figs.  
11 5b and c) as a result of the southwesterly wind field, and under the superposition of the local  
12 pollutant emissions from each city (Li, Du, et al. 2017), the cities on the windward side of the  
13 Taihang Mountains (e.g., HD, SJZ, and BD) quickly developed varying levels of heavy  
14 pollution. In addition, during the AP, due to the large-scale inversion (Figs. 4b, d, f, h) caused  
15 by the rapid temperature rise (Figs. 4a, c, e, g) of the NCP region at upper levels, the  
16 atmospheric stratification was stable, causing the pollutant loading on the NCP (including BJ,  
17 BD, SJZ, HD, LF, CZ, and elsewhere) to increase (Fig. 5d), nearly reaching their pollution  
18 maxima (Fig. 3). Meanwhile, during the RP, affected by the cold air at upper levels (Figs. 4a,



1 c, e, g) from the northwest and the shift in wind direction over the NCP from southwest to  
 2 north, the pollution severity gradually eased from north to south (Fig. 5e), with the air quality  
 3 in the northern part of the region improving significantly (Fig. 5f).

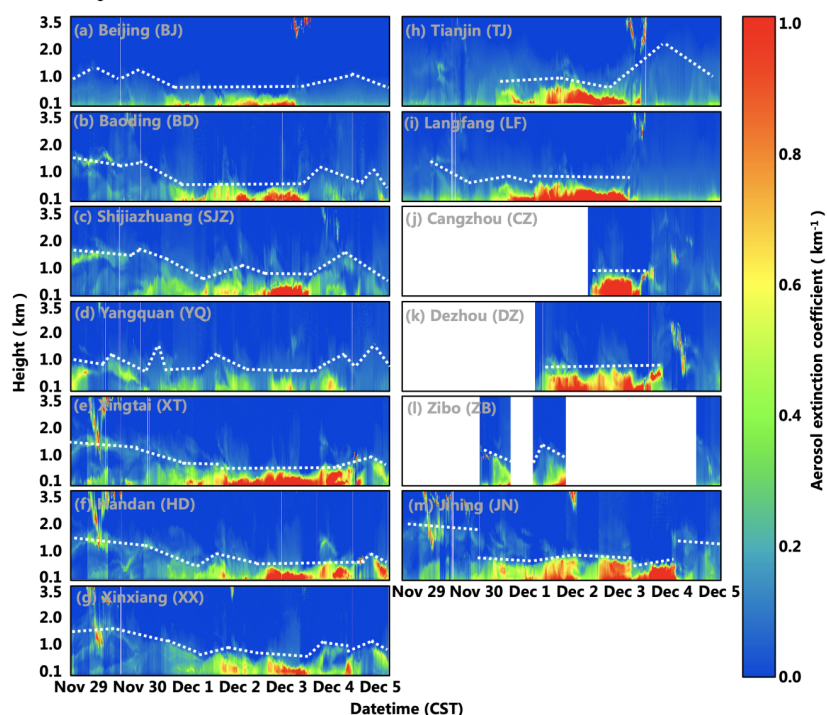


4  
 5 **Figure 5.** Spatial distribution of PM<sub>2.5</sub> in the surface layer during different phases after assimilation.  
 6 The black arrows indicate the wind direction. The circles represent the *in-situ* surface observations.

### 7 3.4 Vertical distribution of aerosols observed by the lidar network

8 In order to quantify the characteristic vertical distribution of aerosols, the observed  
 9 aerosol extinction coefficients from the 13 lidar stations in the NCP were plotted, as shown in  
 10 Fig. 6. These results revealed that on November 29, the aerosol concentration at the surface  
 11 was relatively low, although pollutant transport at heights of 1–2 km (see Figs. 8a, e) occurred  
 12 at six stations (BD, SJZ, YQ, XT, HD, and XX) on the windward side of the Taihang Mountains.  
 13 [Figure S4 demonstrates that these pollutants in the upper air come from the local emissions on](#)  
 14 [the ground, which is due to the updraft lifting to 1-2 km above the ground on the night of](#)  
 15 [November 28.](#) The upper air transport of pollutants continued until December 1, at which it  
 16 merged with the surface flow. Contrary to this, the pollutant transport from north to south  
 17 occurred at a height of 1 km during the RP (e.g., Figs. 6b, d–g). In addition, the atmospheric

1 boundary layer height (ABLH) reached its highest value of the observation period from  
 2 November 29 to 30, averaging more than 1.5 km. The ABLH began to decrease on December  
 3 1, averaging approximately 1 km on that day. The lowest value of the ABLH occurred on  
 4 December 2–3, when its average dropped to less than 0.5 km, making it difficult for pollutants  
 5 to diffuse and causing heavy pollution in the NCP (Li, Guo, et al. 2017). Fortunately, on  
 6 December 4, the atmospheric boundary layer gradually lifted, which was conducive to the  
 7 diffusion of pollutants.



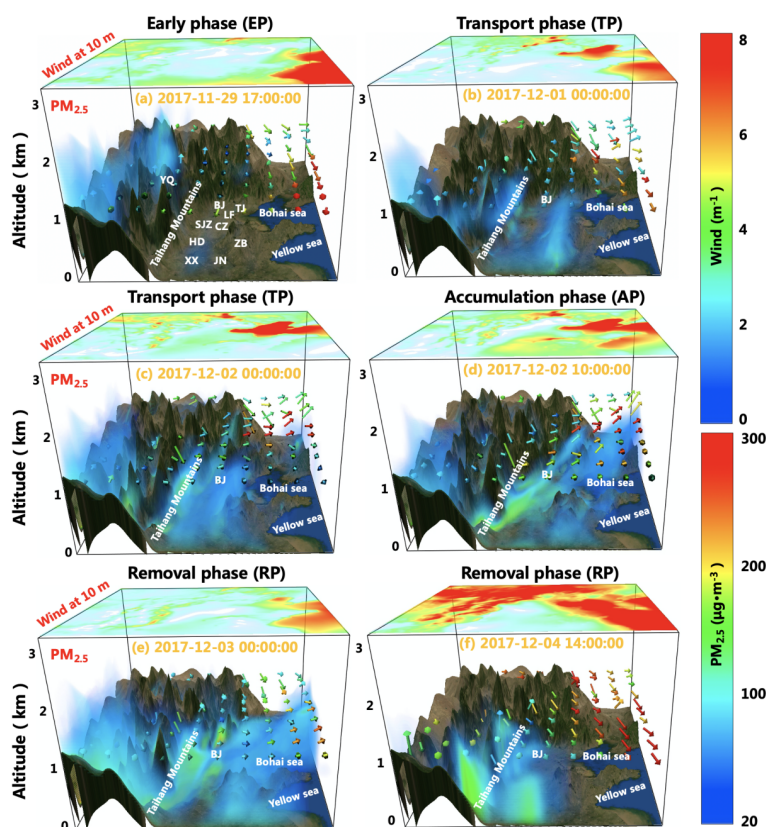
8  
 9 **Figure 6.** Time series of vertical distributions of the aerosol extinction coefficient observed on the  
 10 North China Plain from November 29–December 5, 2017. The white dashed lines represent the  
 11 approximate atmospheric boundary layer height. Missing datasets are plotted in white.

### 12 3.5 Dynamic 3-D evolution of the PM<sub>2.5</sub> concentrations

13 Figure 7 presents the 3-D distribution of PM<sub>2.5</sub> after assimilation, which clearly shows  
 14 the generation, dissipation, transport, and diffusion characteristics of pollutants in the  
 15 atmosphere. The tops of the boxes in the figure depict the wind speeds 10 m above the surface.  
 16 During the EP, the high-concentration pollutants only occurred in the upper air within ~1 km  
 17 of the surface in SX Province (e.g., YQ). During the TP, the high-concentration pollutants were



1 mainly found on the windward side of the Taihang Mountains (southwest pathway), and the  
 2 loading height of  $PM_{2.5}$  was  $< 1$  km, which is illustrated in Fig. 8. During the AP, the average  
 3 concentration of pollutants  $> 200 \mu\text{g}\cdot\text{m}^{-3}$  mainly occurred near the surface. Meanwhile, the  
 4 pollutants with low concentrations at upper levels could be transported to the Bohai Sea.  
 5 During the RP, high-concentration pollutants  $> 100 \mu\text{g}\cdot\text{m}^{-3}$  simultaneously occurred over the  
 6 Bohai Sea and the Yellow Sea.



7  
 8 **Figure 7.** Three-dimensional distribution of  $PM_{2.5}$  during different phases after assimilation. Colors  
 9 within the boxes depict the  $PM_{2.5}$  concentrations. The color-coded arrows represent the wind direction  
 10 and speed at 1 km. On the tops of the boxes, the spatial distributions of wind speed at 10 m are plotted.

### 11 3.6 Quantification of regional transport of $PM_{2.5}$

12 To evaluate the variation of pollutants along different transport pathways at different  
 13 stages, we plotted the vertical profile of the  $PM_{2.5}$  cross-section along the main pollution  
 14 pathways of Beijing coming from the four directions of southwest, south, southeast, and east

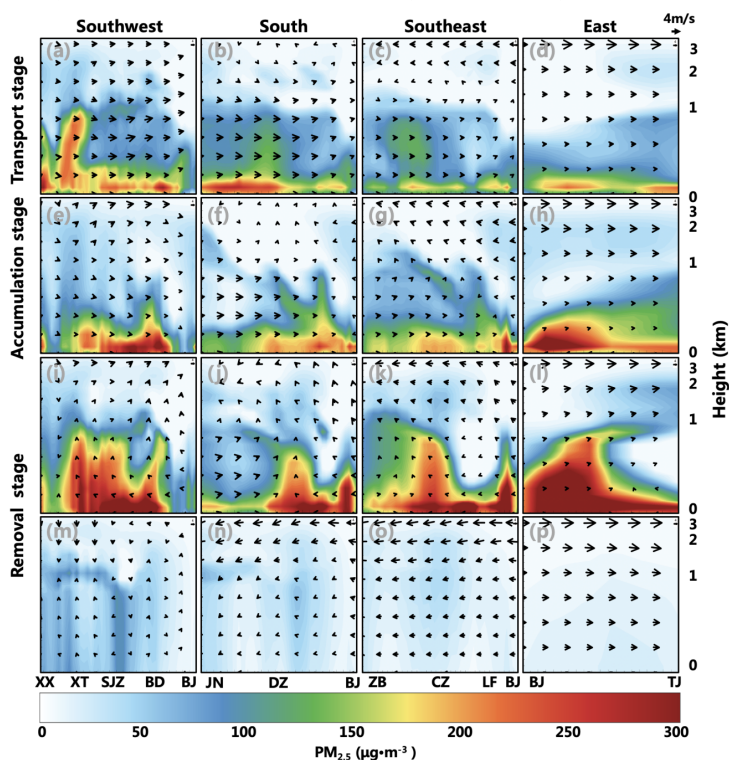
Deleted: come

1 (see Figs. 1b, d). As shown in Fig.8, at XX and XT (located at the start of the southwest  
 2 transport pathway, Fig. 8a), the PM<sub>2.5</sub> concentration is more than 200 μg·m<sup>-3</sup> at a height of 1  
 3 km (Fig. 8a), and the surface PM<sub>2.5</sub> concentration at JN (located in the south pathway) also  
 4 exceeds 200 μg·m<sup>-3</sup> (Fig. 8b). These high concentrations of pollutants were transported to SJZ,  
 5 BD, LF, BJ, and other cities via southwest winds (Figs. 8e, f, g). At the same time, vertical  
 6 downdrafts reduced the height of loading of aerosol layer to ~0.6 km (Fig. 8e). Different from  
 7 the southern (including southwest, south, and southeast) transport pathways, the pollutants in  
 8 TJ were mainly from BJ outflow in all stages of the eastern transport pathways (Figs. 8d, h, l,  
 9 p). In addition, wind direction inconsistencies at the origin (XX, JN, and ZB) and target location  
 10 (Beijing) of the transport pathways occurred at the beginning of the removal phase (Figs. 8i-  
 11 k), which may have been due to the southward delay of the northerly air flow.

Deleted:

Deleted: concentraiton

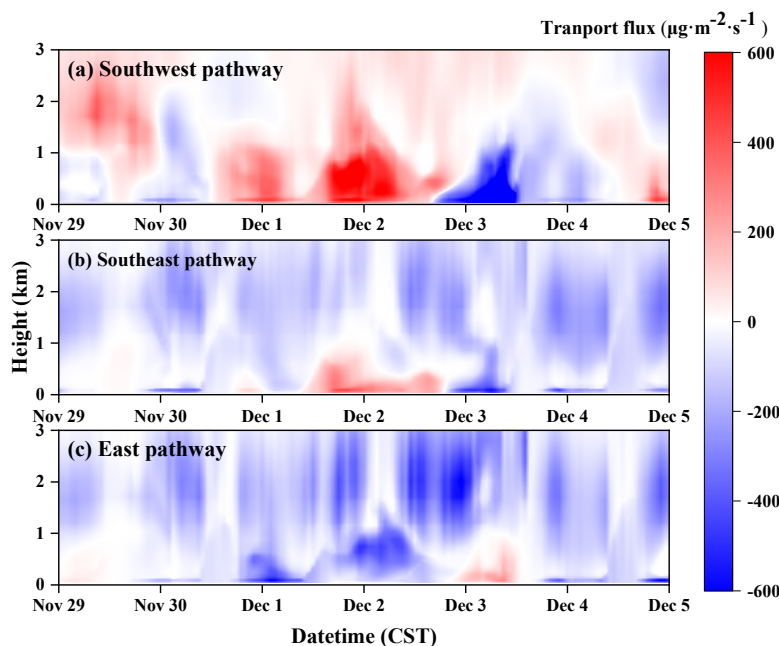
Deleted: aersol



12  
 13 **Figure 8.** Vertical profiles of PM<sub>2.5</sub> cross-sections with wind vectors along the transport pathways,  
 14 including southwest (first column), south (second column), southeast (third column), and east (fourth  
 15 column). The first row (00:00 December 2, 2017) represents the transport stage, the second row (10:00  
 16 December 2, 2017) represents the accumulation stage, the third row (00:00, December 3, 2017) and the  
 17 fourth row (14:00, December 4, 2017) represent the removal stage.

Deleted: 1.5

1 To investigate the vertical variation of PM<sub>2.5</sub> inflow or outflow at different heights and  
2 determine the height at which the main transport occurred (Zhang, Cheng, et al. 2019), we  
3 plotted the vertical distribution of PM<sub>2.5</sub> transport flux in different directions (Fig. 9). Here the  
4 PM<sub>2.5</sub> transport flux is defined as the product of PM<sub>2.5</sub> mass concentration ( $\mu\text{g m}^{-3}$ ), wind speed  
5 ( $\text{m s}^{-1}$ ), and wind direction projection in the current pathway (Xiang et al. 2020). The southwest,  
6 southeast, and east pathways in Fig. 9 were represented by BD, LF, and TJ, respectively, which  
7 are the three lidar stations closest to BJ (Fig. 1). TF > 0 indicates that the pollutants were  
8 imported to Beijing, while TF < 0 indicates that the pollutants were exported from Beijing. The  
9 results revealed that below the height of 3 km, the order of the maximum values of imported  
10 pollutants to Beijing direction was southwest pathway ( $1122.8 \mu\text{g m}^{-2} \text{s}^{-1}$ ) > southeast pathway  
11 ( $423.6 \mu\text{g m}^{-2} \text{s}^{-1}$ ) > east pathway ( $278.3 \mu\text{g m}^{-2} \text{s}^{-1}$ ), while the exported pollutants from Beijing  
12 direction was southwest pathway ( $-1571.4 \mu\text{g m}^{-2} \text{s}^{-1}$ ) > east pathway ( $-877.7 \mu\text{g m}^{-2} \text{s}^{-1}$ ) >  
13 southeast pathway ( $-772.4 \mu\text{g m}^{-2} \text{s}^{-1}$ ). Compared with the PM<sub>2.5</sub> transport flux on the ground  
14 surface, the relatively high value ( $\sim 200 \mu\text{g m}^{-2} \text{s}^{-1}$ ) in the southwest pathway (Fig. 9a) occurred  
15 on November 29 and early morning on December 4, while the relatively extreme value ( $\sim -400$   
16  $\mu\text{g m}^{-2} \text{s}^{-1}$ ) on the east pathway (Fig. 9c) was recorded at the night of December 2.



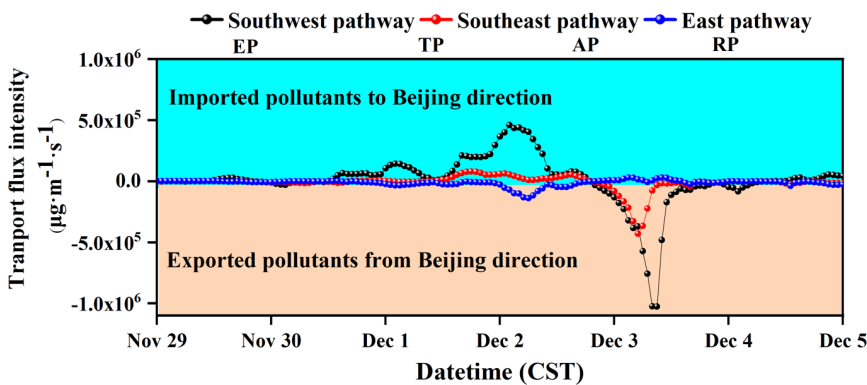
17 **Figure 9.** Time series of PM<sub>2.5</sub> transport flux from different transport pathways. The corresponding  
18 directions of the southwest, southeast, and east pathways are shown in Fig. 1.  
19

1 To further obtain insights into the total transport characteristics in the target area (BJ)  
 2 and its surrounding area (BD, LF, and TJ) during different evolutionary stages, the time series  
 3 of the PM<sub>2.5</sub> transport flux intensity (TFI) was shown in Fig. 10. ~~The TFI was calculated by~~  
 4 ~~integrating the PM<sub>2.5</sub> transport flux from the ground to a certain height, and the height was~~  
 5 ~~selected as 1.5 km, which is consistent with the main transport height of pollutants (Fig. 8) and~~  
 6 ~~the height of boundary layer (Fig. 7).~~ The TFI of PM<sub>2.5</sub> further reveals that pollutants imported  
 7 into the Beijing area with a maximum PM<sub>2.5</sub> TFI of  $\sim 4.6 \times 10^5 \mu\text{g}\cdot\text{m}^{-1}\cdot\text{s}^{-1}$  were transported  
 8 mainly via the southwest pathway during the TP, while the extreme TFI of pollutants exported  
 9 from Beijing via the east pathway was approximately  $-1.4 \times 10^5 \mu\text{g}\cdot\text{m}^{-1}\cdot\text{s}^{-1}$ . In addition, during  
 10 the RP, the pollutants from Beijing were exported to the southwest and southeast, with extreme  
 11 values of approximately  $-1.03 \times 10^6$  and  $-4.3 \times 10^5 \mu\text{g}\cdot\text{m}^{-1}\cdot\text{s}^{-1}$ , respectively. ~~In contrast,~~ the  
 12 absolute value of TFI on the southwest pathway was  $< \sim 1.0 \times 10^4 \mu\text{g}\cdot\text{m}^{-1}\cdot\text{s}^{-1}$  during the EP (Fig.  
 13 10), which indicates that there was no significant inflow or outflow of pollutants. However,  
 14 this reason was mainly due to the offsetting of the inflow of pollutants in the upper-air and the  
 15 outflow of pollutants near the ground (Fig. 9a). This special phenomenon also demonstrates  
 16 that the study of vertical distribution of pollutants has great significance, which can better  
 17 explain the transport characteristics (Zhang, Cheng, et al. 2019).

Deleted: , which

Deleted: within the height range of 1.5 km

Deleted: On the contrary



18  
 19 **Figure 10.** Time series of PM<sub>2.5</sub> transport flux intensity from different transport pathways. The  
 20 corresponding directions of the southwest, southeast, and east pathways are shown in Fig. 1.

## 21 4 Conclusions

22 Accurate quantification of the distribution of particulate matter in the atmosphere is a  
 23 key requirement for predicting air quality and estimating atmospheric environmental capacity  
 24 from atmospheric observations. We utilized a vertical observation network composed of 13

1 aerosol lidars, combined with data assimilation technology, to improve the simulation accuracy  
2 of PM<sub>2.5</sub>, and further analyzed the multi-dimensional evolutionary characteristics of pollutants  
3 in the surface layer, vertical layer, and 3-D space, thereby providing effective data support for  
4 clarifying the spatial transport characteristics of heavy pollution.

5 We found that the average height of the atmospheric boundary layer was < 0.5 km  
6 during the HAP period. We further demonstrated that the transport of pollutants in the NCP  
7 region was mainly via three pathways: southwest, southeast, and east. During the TP, the PM<sub>2.5</sub>  
8 advected into Beijing with a maximum transport flux intensity (TFI) of  $\sim 4.6 \times 10^5 \mu\text{g} \cdot \text{m}^{-1} \cdot \text{s}^{-1}$   
9 was mainly via the southwest pathway, while the polluted air mass in the RP dissipated from  
10 Beijing via the southwest and southeast pathways, with extreme PM<sub>2.5</sub> TFI values of  
11 approximately  $-1.03 \times 10^6$  and  $-4.3 \times 10^5 \mu\text{g} \cdot \text{m}^{-1} \cdot \text{s}^{-1}$ , respectively. In addition, the transport of  
12 regional pollutants to the Yangtze River Delta was due to the continuous southward flow of  
13 northwest and northeast winds. Our results directly revealed that pollutants in the North China  
14 Plain can be transported to the Yellow Sea and the Bohai Sea, providing a dataset for a further  
15 in-depth study of the mechanism of air pollution in the coastal areas of eastern China. This  
16 study also captured the regional transport of air pollutants stretching over 1000 km, proving  
17 the necessity and importance of the joint prevention and control of regional air pollution.

#### 18 **Data availability**

19 The FNL data are available from the following website  
20 (<https://rda.ucar.edu/datasets/ds083.2/>). The data in this study are analyzed using the NCAR  
21 Command Language (<http://www.ncl.ucar.edu/>). The authors are gratefully acknowledging the  
22 China National Environmental Monitoring Center for providing monitoring data for the PM<sub>2.5</sub>  
23 (<http://106.37.208.233:20035>). The lidar data in this study are available upon request from the  
24 corresponding author (yxiang@ahu.edu.cn).

#### 25 **Author contributions**

26 YX and TZ designed this study. YX wrote the manuscript; YC and CM edited it. LL  
27 and TZ helped to analyze the data. YC, CM, WL, and JL provided constructive comments on  
28 this study. All authors contributed to the discussion and final version of the manuscript.

#### 29 **Competing interests**

30 The authors declare that they have no conflict of interest.

## 1 Acknowledgements

2 This work was supported by the National Natural Science Foundation of China  
3 (42005106, 41941011), and the National Key Project of MOST (2017YFC0213002,  
4 2018YFC0213101, 2018YFC0213106, 2018YFC0213201), and the Major science and  
5 technology projects of Anhui Province (No.18030801111), and the Natural Science Foundation  
6 of Anhui Province, China (1908085QD160, 1908085QD170), and the Doctoral Scientific  
7 Research Foundation of Anhui University (Y040418190). The authors are grateful to the China  
8 National Environmental Monitoring Center for providing the PM<sub>2.5</sub> monitoring data. [The](#)  
9 [authors acknowledge the High-performance Computing Platform of Anhui University for](#)  
10 [providing computing resources](#). The authors also gratefully acknowledge © Google Earth for  
11 providing the map used in this research. Yafang Cheng and Chaoqun Ma thank the Minerva  
12 program of Max Planck Society.

## 13 References

- 14 [Barrera, Y. D., T. Nehr Korn, J. Hegarty, M. Sargent, J. Benmergui, E. Gottlieb, S. C. Wofsy,](#)  
15 [P. DeCola, L. Hutyrá, and T. Jones. 2019. 'Using Lidar Technology To Assess Urban](#)  
16 [Air Pollution and Improve Estimates of Greenhouse Gas Emissions in Boston',](#)  
17 [Environmental Science & Technology, 53: 8957-66.](#)
- 18 [Bocquet, M., H. Elbern, H. Eskes, M. Hirtl, R. Zabkar, G. R. Carmichael, J. Flemming, A.](#)  
19 [Inness, M. Pagowski, J. L. P. Camano, P. E. Saide, R. San Jose, M. Sofiev, J. Vira, A.](#)  
20 [Baklanov, C. Carnevale, G. Grell, and C. Seigneur. 2015. 'Data assimilation in](#)  
21 [atmospheric chemistry models: current status and future prospects for coupled](#)  
22 [chemistry meteorology models', Atmospheric Chemistry And Physics, 15: 5325-58.](#)
- 23 [Cao, F., Y. L. Zhang, L. J. Ren, J. W. Liu, J. Li, G. Zhang, D. Liu, Y. L. Sun, Z. F. Wang, Z.](#)  
24 [B. Shi, and P. Q. Fu. 2017. 'New insights into the sources and formation of](#)  
25 [carbonaceous aerosols in China: potential applications of dual-carbon isotopes',](#)  
26 [National Science Review, 4: 804-+.](#)
- 27 [Chatani, S., T. Morikawa, S. Nakatsuka, S. Matsunaga, and H. Minoura. 2011. 'Development](#)  
28 [of a framework for a high-resolution, three-dimensional regional air quality simulation](#)  
29 [and its application to predicting future air quality over Japan', Atmospheric](#)  
30 [Environment, 45: 1383-93.](#)
- 31 [Che, Huizheng, Ke Gui, Xiangao Xia, Yaqiang Wang, Brent N. Holben, Philippe Goloub,](#)  
32 [Emilio Cuevas-Agulló, Hong Wang, Yu Zheng, Hujia Zhao, and Xiaoye Zhang. 2019.](#)  
33 ['Large contribution of meteorological factors to inter-decadal changes in regional](#)  
34 [aerosol optical depth', Atmospheric Chemistry And Physics, 19: 10497-523.](#)
- 35 [Che, Huizheng, Xiangao Xia, Hujia Zhao, Oleg Dubovik, Brent N. Holben, Philippe Goloub,](#)  
36 [Emilio Cuevas-Agulló, Victor Estelles, Yaqiang Wang, Jun Zhu, Bing Qi, Wei Gong,](#)  
37 [Honglong Yang, Renjian Zhang, Leiku Yang, Jing Chen, Hong Wang, Yu Zheng, Ke](#)  
38 [Gui, Xiaochun Zhang, and Xiaoye Zhang. 2019. 'Spatial distribution of aerosol](#)  
39 [microphysical and optical properties and direct radiative effect from the China Aerosol](#)  
40 [Remote Sensing Network', Atmospheric Chemistry And Physics, 19: 11843-64.](#)

Field Code Changed

Deleted: ¶

- 1 Chen, D., Z. Q. Liu, J. M. Ban, and M. Chen. 2019. 'The 2015 and 2016 wintertime air pollution  
2 in China: SO<sub>2</sub> emission changes derived from a WRF-Chem/EnKF coupled data  
3 assimilation system', *Atmospheric Chemistry And Physics*, 19: 8619-50.
- 4 Chen, D. S., X. X. Liu, J. L. Lang, Y. Zhou, L. Wei, X. T. Wang, and X. R. Guo. 2017.  
5 'Estimating the contribution of regional transport to PM<sub>2.5</sub> air pollution in a rural area  
6 on the North China Plain', *Science of the Total Environment*, 583: 280-91.
- 7 Chen, Z., R. Schofield, P. Rayner, T. Zhang, C. Liu, C. Vincent, S. Fiddes, R. G. Ryan, J. Alroe,  
8 Z. D. Ristovski, R. S. Humphries, M. D. Keywood, J. Ward, C. Paton-Walsh, T. Naylor,  
9 and X. Shu. 2019. 'Characterization of aerosols over the Great Barrier Reef: The  
10 influence of transported continental sources', *Science of the Total Environment*, 690:  
11 426-37.
- 12 Cheng, X., Y. Liu, X. Xu, W. You, Z. Zang, L. Gao, Y. Chen, D. Su, and P. Yan. 2019. 'Lidar  
13 data assimilation method based on CRTM and WRF-Chem models and its application  
14 in PM<sub>2.5</sub> forecasts in Beijing', *Science Of the Total Environment*, 682: 541-52.
- 15 Cheng, Y. F., G. J. Zheng, C. Wei, Q. Mu, B. Zheng, Z. B. Wang, M. Gao, Q. Zhang, K. B.  
16 He, G. Carmichael, U. Poschl, and H. Su. 2016. 'Reactive nitrogen chemistry in aerosol  
17 water as a source of sulfate during haze events in China', *Science Advances*, 2,e1601530.
- 18 Collis, Ronald T. H, Frederick G Fernald, and Myron G. H Ligda. 1964. 'Laser Radar Echoes  
19 from a Stratified Clear Atmosphere', *Nature*.
- 20 Dong, Z., S. Wang, J. Xing, X. Chang, D. Ding, and H. Zheng. 2020. 'Regional transport in  
21 Beijing-Tianjin-Hebei region and its changes during 2014-2017: The impacts of  
22 meteorology and emission reduction', *Science of the Total Environment*, 737: 139792.
- 23 Elbern, H., A. Strunk, H. Schmidt, and O. Talagrand. 2007. 'Emission rate and chemical state  
24 estimation by 4-dimensional variational inversion', *Atmospheric Chemistry And  
25 Physics*, 7: 3749-69.
- 26 Fan, W. Z., K. Qin, J. Xu, L. M. Yuan, D. Li, Z. Jin, and K. F. Zhang. 2019. 'Aerosol vertical  
27 distribution and sources estimation at a site of the Yangtze River Delta region of China',  
28 *Atmospheric Research*, 217: 128-36.
- 29 Fernald, F. G. 1984. 'Analysis of Atmospheric Lidar Observations - Some Comments', *Applied  
30 Optics*, 23: 652-53.
- 31 Gao, J. H., A. Woodward, S. Vardoulakis, S. Kovats, P. Wilkinson, L. P. Li, L. Xu, J. Li, J.  
32 Yang, J. Li, L. Cao, X. B. Liu, H. X. Wu, and Q. Y. Liu. 2017. 'Haze, public health and  
33 mitigation measures in China: A review of the current evidence for further policy  
34 response', *Science of the Total Environment*, 578: 148-57.
- 35 Gao, M., P. E. Saide, J. Y. Xin, Y. S. Wang, Z. R. Liu, Y. X. Wang, Z. F. Wang, M. Pagowski,  
36 S. K. Guttikunda, and G. R. Carmichael. 2017. 'Estimates of Health Impacts and  
37 Radiative Forcing in Winter Haze in Eastern China through Constraints of Surface  
38 PM<sub>2.5</sub> Predictions', *Environmental Science & Technology*, 51: 2178-85.
- 39 Heese, B., H. Baars, S. Bohmann, D. Althausen, and R. R. Deng. 2017. 'Continuous vertical  
40 aerosol profiling with a multi-wavelength Raman polarization lidar over the Pearl River  
41 Delta, China', *Atmospheric Chemistry And Physics*, 17: 6679-91.
- 42 Hong, Q. Q., C. Liu, K. L. Chan, Q. H. Hu, Z. Q. Xie, H. R. Liu, F. Q. Si, and J. G. Liu. 2018.  
43 'Ship-based MAX-DOAS measurements of tropospheric NO<sub>2</sub>, SO<sub>2</sub>, and HCHO  
44 distribution along the Yangtze River', *Atmospheric Chemistry And Physics*, 18: 5931-  
45 51.
- 46 Hu, M., S. Guo, J. F. Peng, and Z. J. Wu. 2015. 'Insight into characteristics and sources of  
47 PM<sub>2.5</sub> in the Beijing-Tianjin-Hebei region, China', *National Science Review*, 2: 257-  
48 58.
- 49 Hua, Y., Z. Cheng, S. X. Wang, J. K. Jiang, D. R. Chen, S. Y. Cai, X. Fu, Q. Y. Fu, C. H. Chen,  
50 B. Y. Xu, and J. Q. Yu. 2015. 'Characteristics and source apportionment of PM<sub>2.5</sub>

1 during a fall heavy haze episode in the Yangtze River Delta of China', *Atmospheric*  
2 *Environment*, 123: 380-91.

3 Huang, M., J. H. Crawford, G. S. Diskin, J. A. Santanello, S. V. Kumar, S. E. Pusede, M.  
4 Parrington, and G. R. Carmichael. 2018. 'Modeling Regional Pollution Transport  
5 Events During KORUS-AQ: Progress and Challenges in Improving Representation of  
6 Land-Atmosphere Feedbacks', *Journal Of Geophysical Research-Atmospheres*, 123:  
7 10732-56.

8 Huang, X., L. X. Zhou, A. J. Ding, X. M. Qi, W. Nie, M. H. Wang, X. G. Chi, T. Petaja, V. M.  
9 Kerminen, P. Roldin, A. Rusanen, M. Kulmala, and M. Boy. 2016. 'Comprehensive  
10 modelling study on observed new particle formation at the SORPES station in Nanjing,  
11 China', *Atmospheric Chemistry And Physics*, 16: 2477-92.

12 Huang, Xin, Zilin Wang, and Aijun Ding. 2018. 'Impact of Aerosol-PBL Interaction on Haze  
13 Pollution: Multiyear Observational Evidences in North China', *Geophysical Research*  
14 *Letters*, 45: 8596-603.

15 Jiang, Z. Q., Z. Q. Liu, T. J. Wang, C. S. Schwartz, H. C. Lin, and F. Jiang. 2013. 'Probing into  
16 the impact of 3DVAR assimilation of surface PM10 observations over China using  
17 process analysis', *Journal of Geophysical Research-Atmospheres*, 118: 6738-49.

18 Klett, J. D. 1981. 'Stable Analytical Inversion Solution for Processing Lidar Returns', *Applied*  
19 *Optics*, 20: 211-20.

20 Kumar, M., M. P. Raju, R. K. Singh, A. K. Singh, R. S. Singh, and T. Banerjee. 2017.  
21 'Wintertime characteristics of aerosols over middle Indo-Gangetic Plain: Vertical  
22 profile, transport and radiative forcing', *Atmospheric Research*, 183: 268-82.

23 Li, J., H. Y. Du, Z. F. Wang, Y. L. Sun, W. Y. Yang, J. J. Li, X. Tang, and P. Q. Fu. 2017.  
24 'Rapid formation of a severe regional winter haze episode over a mega-city cluster on  
25 the North China Plain', *Environmental Pollution*, 223: 605-15.

26 Li, X., Q. Zhang, Y. Zhang, L. Zhang, Y. X. Wang, Q. Q. Zhang, M. Li, Y. X. Zheng, G. N.  
27 Geng, T. J. Wallington, W. J. Han, W. Shen, and K. B. He. 2017. 'Attribution of PM2.5  
28 exposure in Beijing-Tianjin-Hebei region to emissions: implication to control  
29 strategies', *Science Bulletin*, 62: 957-64.

30 Li, Y. R., C. X. Ye, J. Liu, Y. Zhu, J. X. Wang, Z. Q. Tan, W. L. Lin, L. M. Zeng, and T. Zhu.  
31 2016. 'Observation of regional air pollutant transport between the megacity Beijing and  
32 the North China Plain', *Atmospheric Chemistry And Physics*, 16: 14265-83.

33 Li, Z. Q., J. P. Guo, A. J. Ding, H. Liao, J. J. Liu, Y. L. Sun, T. J. Wang, H. W. Xue, H. S.  
34 Zhang, and B. Zhu. 2017. 'Aerosol and boundary-layer interactions and impact on air  
35 quality', *National Science Review*, 4: 810-33.

36 Liu, Z. Q., Q. H. Liu, H. C. Lin, C. S. Schwartz, Y. H. Lee, and T. J. Wang. 2011. 'Three-  
37 dimensional variational assimilation of MODIS aerosol optical depth: Implementation  
38 and application to a dust storm over East Asia', *Journal of Geophysical Research-*  
39 *Atmospheres*, 116.

40 Lu, L. H., W. Q. Liu, T. S. Zhang, Y. H. Lu, Y. S. Dong, Z. Y. Chen, G. Q. Fan, and S. S. Qi.  
41 2015. 'Two Data Inversion Algorithms of Aerosol Horizontal Distribution Detected by  
42 MPL and Error Analysis', *Spectroscopy and Spectral Analysis*, 35: 1774-78.

43 Lv, L. H., W. Q. Liu, T. S. Zhang, Z. Y. Chen, Y. S. Dong, G. Q. Fan, Y. Xiang, Y. W. Yao,  
44 N. Yang, B. L. Chu, M. Teng, and X. W. Shu. 2017a. 'Observations of particle  
45 extinction, PM2.5 mass concentration profile and flux in north China based on mobile  
46 lidar technique', *Atmospheric Environment*, 164: 360-69.

47 Lv, Lihui, Wenqing Liu, Tianshu Zhang, Zhenyi Chen, Yunsheng Dong, Guangqiang Fan, Yan  
48 Xiang, Yawei Yao, Nan Yang, Baolin Chu, Man Teng, and Xiaowen Shu. 2017b.  
49 'Observations of particle extinction, PM 2.5 mass concentration profile and flux in north  
50 China based on mobile lidar technique', *Atmospheric Environment*.



- 1 Ma, C. Q., T. J. Wang, A. P. Mizzi, J. L. Anderson, B. L. Zhuang, M. Xie, and R. S. Wu. 2019.  
2 'Multiconstituent Data Assimilation With WRF-Chem/DART: Potential for Adjusting  
3 Anthropogenic Emissions and Improving Air Quality Forecasts Over Eastern China',  
4 *Journal Of Geophysical Research-Atmospheres*, 124: 7393-412.
- 5 Ma, C. Q., T. J. Wang, Z. L. Zang, and Z. J. Li. 2018. 'Comparisons of Three-Dimensional  
6 Variational Data Assimilation and Model Output Statistics in Improving Atmospheric  
7 Chemistry Forecasts', *Advances In Atmospheric Sciences*, 35: 813-25.
- 8 Pagowski, M., Z. Liu, G. A. Grell, M. Hu, H. C. Lin, and C. S. Schwartz. 2014. 'Implementation  
9 of aerosol assimilation in Gridpoint Statistical Interpolation (v. 3.2) and WRF-Chem  
10 (v. 3.4.1)', *Geoscientific Model Development*, 7: 1621-27.
- 11 Pang, J. M., Z. Q. Liu, X. M. Wang, J. Bresch, J. M. Ban, D. Cnen, and J. Kim. 2018.  
12 'Assimilating AOD retrievals from GOCI and VIIRS to forecast surface PM2.5  
13 episodes over Eastern China', *Atmospheric Environment*, 179: 288-304.
- 14 Parrish, David F., and John C. Derber. 1992. 'The National Meteorological Center's Spectral  
15 Statistical-Interpolation Analysis System', *Monthly Weather Review*, 120: 1747-63.
- 16 Pokharel, Manisha, Jie Guang, Bin Liu, Shichang Kang, Yaoming Ma, Brent N. Holben,  
17 Xiang'ao Xia, Jinyuan Xin, Kirpa Ram, Dipesh Rupakheti, Xin Wan, Guangming Wu,  
18 Hemraj Bhattarai, Chuanfeng Zhao, and Zhiyuan Cong. 2019. 'Aerosol Properties Over  
19 Tibetan Plateau From a Decade of AERONET Measurements: Baseline, Types, and  
20 Influencing Factors', *Journal of Geophysical Research: Atmospheres*, 124: 13357-74.
- 21 Saide, P. E., G. R. Carmichael, Z. Liu, C. S. Schwartz, H. C. Lin, A. M. da Silva, and E. Hyer.  
22 2013. 'Aerosol optical depth assimilation for a size-resolved sectional model: impacts  
23 of observationally constrained, multi-wavelength and fine mode retrievals on regional  
24 scale analyses and forecasts', *Atmospheric Chemistry And Physics*, 13: 10425-44.
- 25 Saide, P. E., J. Kim, C. H. Song, M. Choi, Y. F. Cheng, and G. R. Carmichael. 2014.  
26 'Assimilation of next generation geostationary aerosol optical depth retrievals to  
27 improve air quality simulations', *Geophysical Research Letters*, 41: 9188-96.
- 28 Schwartz, C. S., Z. Q. Liu, H. C. Lin, and S. A. McKeen. 2012. 'Simultaneous three-  
29 dimensional variational assimilation of surface fine particulate matter and MODIS  
30 aerosol optical depth', *Journal Of Geophysical Research-Atmospheres*, 117.
- 31 Sheng, Z. Z., H. Z. Che, Q. L. Chen, X. A. Xia, D. Liu, Z. Z. Wang, H. J. Zhao, K. Gui, Y.  
32 Zheng, T. Z. Sun, X. P. Li, C. Liu, H. Wang, Y. Q. Wang, and X. Y. Zhang. 2019.  
33 'Aerosol vertical distribution and optical properties of different pollution events in  
34 Beijing in autumn 2017', *Atmospheric Research*, 215: 193-207.
- 35 Su, H., Y. Cheng, and U. Poschl. 2020. 'New Multiphase Chemical Processes Influencing  
36 Atmospheric Aerosols, Air Quality, and Climate in the Anthropocene', *Acc Chem Res*.
- 37 Sun, Jinjin, Lin Huang, Hong Liao, Jingyi Li, and Jianlin Hu. 2017. 'Impacts of Regional  
38 Transport on Particulate Matter Pollution in China: a Review of Methods and Results',  
39 *Current Pollution Reports*, 3: 182-91.
- 40 Tao, W., H. Su, G. Zheng, J. Wang, C. Wei, L. Liu, N. Ma, M. Li, Q. Zhang, U. Pöschl, and  
41 Y. Cheng. 2020. 'Aerosol pH and chemical regimes of sulfate formation in aerosol  
42 water during winter haze in the North China Plain', *Atmos. Chem. Phys. Discuss.*, 2020:  
43 1-31.
- 44 Tao, Z. M., Z. Z. Wang, S. J. Yang, H. H. Shan, X. M. Ma, H. Zhang, S. G. Zhao, D. Liu, C.  
45 B. Xie, and Y. J. Wang. 2016. 'Profiling the PM2.5 mass concentration vertical  
46 distribution in the boundary layer', *Atmospheric Measurement Techniques*, 9: 1369-76.
- 47 Tian, P. F., X. J. Cao, L. Zhang, N. X. Sun, L. Sun, T. Logan, J. S. Shi, Y. Wang, Y. M. Ji, Y.  
48 Lin, Z. W. Huang, T. Zhou, Y. Y. Shi, and R. Y. Zhang. 2017. 'Aerosol vertical  
49 distribution and optical properties over China from long-term satellite and ground-  
50 based remote sensing', *Atmospheric Chemistry And Physics*, 17: 2509-23.

- 1 Wang, J., M. Zhang, X. Bai, H. Tan, S. Li, J. Liu, R. Zhang, M. A. Wolters, X. Qin, M. Zhang,  
2 H. Lin, Y. Li, J. Li, and L. Chen. 2017. 'Large-scale transport of PM2.5 in the lower  
3 troposphere during winter cold surges in China', *Sci Rep*, 7: 13238.
- 4 Wang, L. L., J. K. Liu, Z. Q. Gao, Y. B. Li, M. Huang, S. H. Fan, X. Y. Zhang, Y. J. Yang, S.  
5 G. Miao, H. Zou, Y. L. Sun, Y. Chen, and T. Yang. 2019. 'Vertical observations of the  
6 atmospheric boundary layer structure over Beijing urban area during air pollution  
7 episodes', *Atmospheric Chemistry And Physics*, 19: 6949-67.
- 8 Wang, L. L., Z. R. Liu, Y. Sun, D. S. Ji, and Y. S. Wang. 2015. 'Long-range transport and  
9 regional sources of PM2.5 in Beijing based on long-term observations from 2005 to  
10 2010', *Atmospheric Research*, 157: 37-48.
- 11 Wang, Y., K. N. Sartelet, M. Bocquet, and P. Chazette. 2013. 'Assimilation of ground versus  
12 lidar observations for PM10 forecasting', *Atmospheric Chemistry And Physics*, 13: 269-  
13 83.
- 14 Xiang, Y., T. S. Zhang, J. G. Liu, L. H. Lv, Y. S. Dong, and Z. Y. Chen. 2019. 'Atmosphere  
15 boundary layer height and its effect on air pollutants in Beijing during winter heavy  
16 pollution', *Atmospheric Research*, 215: 305-16.
- 17 Xiang, Yan, Lihui Lv, Wenxuan Chai, Tianshu Zhang, Jianguo Liu, and Wenqing Liu. 2020.  
18 'Using Lidar technology to assess regional air pollution and improve estimates of  
19 PM2.5 transport in the North China Plain', *Environmental Research Letters*, 15: 094071.
- 20 Xu, J. M., L. Y. Chang, Y. H. Qu, F. X. Yan, F. Y. Wang, and Q. Y. Fu. 2016. 'The  
21 meteorological modulation on PM2.5 interannual oscillation during 2013 to 2015 in  
22 Shanghai, China', *Science of the Total Environment*, 572: 1138-49.
- 23 Yang, Xiaowen, Shuiyuan Cheng, Jianbing Li, Jianlei Lang, and Gang Wang. 2017.  
24 'Characterization of Chemical Composition in PM2.5 in Beijing before, during, and  
25 after a Large-Scale International Event', *Aerosol and Air Quality Research*, 17: 896-  
26 907.
- 27 Yuan, R. M., X. Y. Zhang, H. Liu, Y. Gui, B. H. Shao, X. P. Tao, Y. Q. Wang, J. T. Zhong, Y.  
28 B. Li, and Z. Q. Gao. 2019. 'Aerosol vertical mass flux measurements during heavy  
29 aerosol pollution episodes at a rural site and an urban site in the Beijing area of the  
30 North China Plain', *Atmospheric Chemistry And Physics*, 19: 12857-74.
- 31 Yumimoto, K., I. Uno, N. Sugimoto, A. Shimizu, Z. Liu, and D. M. Winker. 2008. 'Adjoint  
32 inversion modeling of Asian dust emission using lidar observations', *Atmospheric  
33 Chemistry And Physics*, 8: 2869-84.
- 34 Zhang, C. X., C. Liu, K. L. Chan, Q. H. Hu, H. R. Liu, B. Li, C. Z. Xing, W. Tan, H. J. Zhou,  
35 F. Q. Si, and J. G. Liu. 2020. 'First observation of tropospheric nitrogen dioxide from  
36 the Environmental Trace Gases Monitoring Instrument onboard the GaoFen-5 satellite',  
37 *Light-Science & Applications*, 9.
- 38 Zhang, C. X., C. Liu, Q. H. Hu, Z. N. Cai, W. J. Su, C. Z. Xia, Y. Z. Zhu, S. W. Wang, and J.  
39 G. Liu. 2019. 'Satellite UV-Vis spectroscopy: implications for air quality trends and  
40 their driving forces in China during 2005-2017', *Light-Science & Applications*, 8.
- 41 Zhang, Hanyu, Shuiyuan Cheng, Sen Yao, Xiaoqi Wang, and Chuanda Wang. 2019. 'Insights  
42 into the temporal and spatial characteristics of PM2.5 transport flux across the district,  
43 city and region in the North China Plain', *Atmospheric Environment*, 218.
- 44 Zhang, Hua, Bing Xie, Shu-Yun Zhao, and Qi Chen. 2014. 'PM2.5 and tropospheric O3 in  
45 China and an analysis of the impact of pollutant emission control', *Advances in Climate  
46 Change Research*, 5: 136-41.
- 47 Zhang, Q., Y. X. Zheng, D. Tong, M. Shao, S. X. Wang, Y. H. Zhang, X. D. Xu, J. N. Wang,  
48 H. He, W. Q. Liu, Y. H. Ding, Y. Lei, J. H. Li, Z. F. Wang, X. Y. Zhang, Y. S. Wang,  
49 J. Cheng, Y. Liu, Q. R. Shi, L. Yan, G. N. Geng, C. P. Hong, M. Li, F. Liu, B. Zheng,  
50 J. J. Cao, A. J. Ding, J. Gao, Q. Y. Fu, J. T. Huo, B. X. Liu, Z. R. Liu, F. M. Yang, K.

1 B. He, and J. M. Hao. 2019. 'Drivers of improved PM2.5 air quality in China from 2013  
2 to 2017', *Proceedings of the National Academy of Sciences of the United States of*  
3 *America*, 116: 24463-69.

4 Zhang, Y. H., H. Su, L. J. Zhong, Y. F. Cheng, L. M. Zeng, X. S. Wang, Y. R. Xiang, J. L.  
5 Wang, D. F. Gao, M. Shao, S. J. Fan, and S. C. Liu. 2008. 'Regional ozone pollution  
6 and observation-based approach for analyzing ozone-precursor relationship during the  
7 PRIDE-PRD2004 campaign', *Atmospheric Environment*, 42: 6203-18.

8 Zhang, Y. L., and F. Cao. 2015. 'Fine particulate matter (PM2.5) in China at a city level',  
9 *Scientific Reports*, 5.

10 Zhang, Y. X., Q. Yuan, D. Huang, S. F. Kong, J. Zhang, X. F. Wang, C. Y. Lu, Z. B. Shi, X.  
11 Y. Zhang, Y. L. Sun, Z. F. Wang, L. Y. Shao, J. H. Zhu, and W. J. Li. 2018. 'Direct  
12 Observations of Fine Primary Particles From Residential Coal Burning: Insights Into  
13 Their Morphology, Composition, and Hygroscopicity', *Journal Of Geophysical*  
14 *Research-Atmospheres*, 123: 12964-79.

15 Zhang, Y., X. Zhang, L. T. Wang, Q. Zhang, F. K. Duan, and K. B. He. 2016. 'Application of  
16 WRF/Chem over East Asia: Part I. Model evaluation and intercomparison with  
17 MM5/CMAQ', *Atmospheric Environment*, 124: 285-300.

18 Zhao, D., G. Liu, J. Xin, J. Quan, Y. Wang, X. Wang, L. Dai, W. Gao, G. Tang, B. Hu, Y. Ma,  
19 X. Wu, L. Wang, Z. Liu, and F. Wu. 2020. 'Haze pollution under a high atmospheric  
20 oxidation capacity in summer in Beijing: insights into formation mechanism of  
21 atmospheric physicochemical processes', *Atmos. Chem. Phys.*, 20: 4575-92.

22 Zheng, G. J., F. K. Duan, H. Su, Y. L. Ma, Y. Cheng, B. Zheng, Q. Zhang, T. Huang, T. Kimoto,  
23 D. Chang, U. Poschl, Y. F. Cheng, and K. B. He. 2015. 'Exploring the severe winter  
24 haze in Beijing: the impact of synoptic weather, regional transport and heterogeneous  
25 reactions', *Atmospheric Chemistry And Physics*, 15: 2969-83.

26 Zheng, M., C. Q. Yan, S. X. Wang, K. B. He, and Y. H. Zhang. 2017. 'Understanding PM2.5  
27 sources in China: challenges and perspectives', *National Science Review*, 4: 801-03.

28 Zheng, Y., H. Z. Che, X. G. Xia, Y. Q. Wang, H. Wang, Y. F. Wu, J. Tao, H. J. Zhao, L. C.  
29 An, L. Li, K. Gui, T. Z. Sun, X. P. Li, Z. Z. Sheng, C. Liu, X. Y. Yang, Y. X. Liang, L.  
30 Zhang, C. Liu, X. Kuang, S. Luo, Y. C. You, and X. Y. Zhang. 2019. 'Five-year  
31 observation of aerosol optical properties and its radiative effects to planetary boundary  
32 layer during air pollution episodes in North China: Intercomparison of a plain site and  
33 a mountainous site in Beijing', *Science of the Total Environment*, 674: 140-58.

34 Zhong, J. T., X. Y. Zhang, Y. Q. Wang, J. Y. Sun, Y. M. Zhang, J. Z. Wang, K. Y. Tan, X. J.  
35 Shen, H. C. Che, L. Zhang, Z. X. Zhang, X. F. Qi, H. R. Zhao, S. X. Ren, and Y. Li.  
36 2017. 'Relative Contributions of Boundary-Layer Meteorological Factors to the  
37 Explosive Growth of PM2.5 during the Red-Alert Heavy Pollution Episodes in Beijing  
38 in December 2016', *Journal of Meteorological Research*, 31: 809-19.

39 Zhou, Y. D., Y. Zhao, P. Mao, Q. Zhang, J. Zhang, L. P. Qiu, and Y. Yang. 2017. 'Development  
40 of a high-resolution emission inventory and its evaluation and application through air  
41 quality modeling for Jiangsu Province, China', *Atmospheric Chemistry and Physics*, 17:  
42 211-33.

43